

Phase-locked Patterns of the Kuramoto Model on 3-Regular Graphs

Lee DeVille¹ and Bard Ermentrout²

¹*Department of Mathematics, University of Illinois*

²*Department of Mathematics, University of Pittsburgh*

We consider the existence of non-synchronized fixed points to the Kuramoto model defined on sparse networks, specifically, networks where each vertex has degree exactly three. We show that “most” such networks support multiple attracting phase-locked solutions that are not synchronized, and study the depth and width of the basins of attraction of these phase-locked solutions. We also show that it is common in “large enough” graphs to find phase-locked solutions where one or more of the links has angle difference greater than $\pi/2$.

PACS numbers: 02.10.Ox, 02.10.Yn, 02.30.Hq, 05.45.Xt, 89.75.Kd, 89.75.-k

I. INTRODUCTION

A. Background

Rhythmic phenomena are ubiquitous in biological and physical systems and are typically modeled as a limit cycle or a network of many coupled oscillators. Networks of coupled oscillators are, in general, difficult to analyze, but, in some cases, it is possible to reduce such networks into similar networks of much simpler models. For example, if coupling is “weak” (in a sense that can be made precise, see e.g. [EK84]) and the individual oscillators are nearly identical, models of the form:

$$x'_i = f(x_i) + \epsilon \sum_{ij} G_{ij}(x_i, x_j), \quad i, j = 1, \dots, N$$

where ϵ is small and $u' = f(u)$ admits an asymptotically stable limit cycle, can be reduced to the study of a system on the N -torus of the form:

$$\theta'_i = \epsilon \sum_j H_{ij}(\theta_j - \theta_i). \quad (1)$$

Here $H_{ij}(\phi)$ are T -periodic functions of ϕ where T is the period of the uncoupled limit cycles and $x_i(t) = u(t + \theta_i) + O(\epsilon)$. When $H_{ij}(\phi) = \omega_i + K_{ij} \sin(\phi)$, we have the so-called Kuramoto model. The particular case when $K_{ij} = 1/N$ and N is large has been the subject of much theory [Str00] and serves as a core model for synchronization phenomena. When K_{ij} is zero except when $|i - j| = 1$, then this represents a network of oscillators in a chain which has been used as a model for swimming of the lamprey [CHR82] and other locomotory pattern generators. More general functions $H_{ij}(\phi)$ were considered in [Erm92] where general conditions for the existence of stable periodic solutions were given.

In this paper, we want to make a distinction between different types of synchronization. In the Kuramoto model, synchrony refers to a state in which there is a collective rhythm or organization that emerges from the infinite sized system. For a finitely sized system, as we study here, we are interested in fully *phase-locked solutions* which correspond to periodic solutions to (1) and

wish to distinguish them from what we will call *synchronous solutions*, where $\theta_i(t) = \theta_j(t)$ for all i, j . As we will formally define below, a phase pattern is a stable phase-locked state that is not synchronized (in the sense above). For example in a four oscillator model for quadruped locomotion [GS06] would call the walk (where each of the oscillators take the four phases, $0, 1/4, 1/2, 3/4$) and the trot (pairs of oscillators are half a cycle out of phase) patterns, but not the pronk (where all oscillators have the same phase, that is, they are synchronized in our sense). A more concrete example can be found in [PE94] where we showed that a square array of nearest neighbor oscillators of the form:

$$\theta'_i = 1 + \sum_{j \in N_i} \sin(\theta_j - \theta_i)$$

could admit both a stable synchronized solution ($\theta_i = t$) or various types of stable rotating waves. The latter are a pattern and the former not. In [UE15] we showed that there was a stable rotating wave on a network of oscillators on the dodecahedral graph and generalizations of it as well as stable synchronization. Nonsynchronized activity in the form of phase-waves is a common feature of spatio-temporal dynamics in the nervous system [EK01]. This patterned activity can arise from either heterogeneities in the medium or from topological defects [PE94, AC13] where all the oscillators are identical. It is the latter types of patterns that we are interested in. We finally note that the same network can often admit multiple stable solutions; such is the case in [PE94, UE15, AC13].

B. Motivation

The main object of study in this paper is the Kuramoto system on sparse graphs, and in particular we concentrate on cubic graphs in this paper. (Recall that a *cubic* graph is a graph which is regular of degree 3, i.e. each node has exactly three neighbors in the graph.) By Kuramoto system, we mean here that the interaction between oscillators is the sine-function: in equation (1) we choose $H_{ij}(\phi) = 1 + c_{ij} \sin(\phi)$ where $C = c_{ij}$ is the

adjacency matrix for an undirected graph. In absence of coupling, all oscillators have the same dynamics. We will use the term “patterns” to refer to non-synchronized stable phase-locked states. The two cases where patterns are well understood are the cases of ring graphs and of the complete graph. The ring graph can support a large number of patterns [WSG06] and the complete graph supports no patterns. Moreover, the patterns on the ring are very easy to characterize. If N is the number of oscillators in the ring, then for any $k < \lfloor N/4 \rfloor$, there is a stable fixed point given by the k -twist solution $\theta_m = 2\pi km/N$. The condition for stability says that the angle difference between any two connected nodes must be between $-\pi/2$ and $\pi/2$.

Since rings are regular of degree 2, cubic graphs are the sparsest regular graphs not yet understood. We might expect that as we add nodes, patterns are easier to find as they were in rings. But of course the situation is more complex: in the case of the ring, we know the size of the (only) cycle in the graph, but a cubic graph will have many cycles and we have to be able to find a set of angles that match around all of these cycles (note that the angle differences around any cycle will need to sum to a multiple of 2π).

We are also particularly interested in studying patterns with long links, by which we mean an edge on which there is an angle difference larger than $\pi/2$. As we discuss below, it is straightforward to show that a pattern that has only short links will be stable, but the converse is not true. Of course, it is easy to obtain a long-link pattern by making the weight on one or more edges particularly weak and allowing it to stretch. But it is not *a priori* clear that it is possible to do so when all of the edge weights have the same magnitude. It was shown in [DeV12] that there are no long-link patterns on the ring when the edge weights are the same, and to the best of our knowledge, it has never been shown that a Kuramoto model where the oscillators have identical frequencies and the edge weights are equal can exhibit a long-link pattern, but in this paper we exhibit many examples of these. (The existence of long-link patterns has been shown on the ring where the edge weights are equal but the intrinsic frequencies are chosen to be different in [BDF].)

C. Definitions

Definition I.1. Let $G = (V, E)$ be a graph and define the **Kuramoto flow on G** as the ODE on $\mathbb{R}^{|V|}$:

$$\frac{d}{dt}\theta_v = \sum_{w \in N(v)} \sin(\theta_w - \theta_v). \quad (2)$$

(Here $N(v)$ is the set of neighbors of the vertex v in the graph.) A **fixed point** or **phase-locked solution** is any point θ which gives a fixed point for this ODE. We assume throughout that the graph G is connected.

Remark I.2. • We assume here that all of the oscillators have the same intrinsic frequency. It is then true that the strength of coupling is irrelevant, so we set it to unity.

- Since the right-hand side of the ODE is invariant under the transformation $\theta \mapsto \theta + c\mathbf{1}$, fixed points are only unique up to translation. We will typically make the convention of choosing a distinguished vertex v and enforcing that $\theta_v = 0$.
- It is clear from inspection that $\theta_v \equiv 0$ is a fixed point of (2) for any graph G . We will always call this the **synchronized** or **sync** solution. Also notice that since the oscillators are assumed to have the same intrinsic frequencies, this system will not have precessing solutions with a moving center of gravity. Summing (2) over v and using the symmetry of the graph we see that the sum of the angles is constant.

Definition I.3. We say that a fixed point θ of (2) is **stable** if the Jacobian at θ has one zero eigenvalue and the remainder negative, and if $\mathbf{1}$ is the eigenvector in the nullspace. The reason for this is that, as is easy to show, $(d/dt)\langle \theta, \mathbf{1} \rangle = 0$ for any solution, and thus we can pick the sum of θ_i a priori and see that it is fixed. Moreover, the motion in the $\mathbf{1}$ direction gives a zero eigenvalue, so if it is unique then the point is dynamically stable in $\mathbf{1}^\perp$.

Every stable fixed point has an open set which is its basin of attraction. We will refer to the **width** of such a basin as its Lebesgue measure on the set $\mathbf{1}^\perp$ inside $[0, 2\pi]^N$.

Proposition 1. The sync solution is always stable.

Proof. We see that the Jacobian of (2) at the sync solution is the $|V| \times |V|$ matrix whose entries are given by

$$J_{vw} = \begin{cases} 1, & v \neq w, (v, w) \in E, \\ 0, & v \neq w, (v, w) \notin E, \\ -\deg(v), & v = w. \end{cases}$$

As such it is the negative of the standard graph Laplacian. As seen in [Chu97], this implies that J is negative semidefinite, and the number of zero eigenvalues is the number of connected components of the graph. In particular, if G is connected, then the Jacobian at zero has exactly one zero eigenvalue, and the remainder are negative. Moreover, $\ker(J) = \text{span}(\mathbf{1})$. \square

Definition I.4. Any stable fixed point of (2) that is not the sync solution is termed a **stable pattern**, or typically just a **pattern**.

Definition I.5. For any graph G , there is a potential energy function

$$\Phi_G(\theta) := \sum_{(v,w) \in E(G)} (1 - \cos(\theta_v - \theta_w)). \quad (3)$$

It is not hard to show that (2) can be written as $\theta' = -\nabla\Phi_G(\theta)$. The **energy** of a solution is just the number $\Phi_G(\theta)$. Notice that the sync solution always has zero energy, and any pattern will have a positive energy.

Definition I.6. Let θ be a pattern for some graph G . For each edge $(v, w) \in E(G)$, we say the link is **long** if $|\theta_v - \theta_w| > \pi/2$, **short** if $|\theta_v - \theta_w| < \pi/2$, and **critical** if $|\theta_v - \theta_w| = \pi/2$.

Remark I.7. The reason for the distinction between short and long is motivated by considerations of stability. Let θ be a fixed point of (2) for a given graph G . Then the Jacobian of the flow at this point is given by

$$J_{vw} = \begin{cases} \cos(\theta_v - \theta_w), & v \neq w, (v, w) \in E, \\ 0, & v \neq w, (v, w) \notin E, \\ -\sum_{u \in V} J_{vu}, & v = w. \end{cases}$$

Note that each row of this matrix is zero sum, so that $J\mathbf{1} = \mathbf{0}$. Moreover, if all of the off-diagonal terms are positive, i.e. all of the links are short, then the standard theory of weighted graph Laplacians [Chu97] tells us that the fixed point is stable. The case where some of the links are short and some are critical is addressed in [Erm92].

When there are long links, i.e. when some of the off-diagonal terms are negative, then there is no assurance that the point is stable. However, the existence of long links is not enough to exclude stability: in [BD14, BDK], the study of weighted Laplacians with signed entries was undertaken and general conditions were found to determine when such Laplacians would be stable. In particular, if there is a configuration with long links such that every vertex is connected by a path of short links, then it is possible that this gives a stable point.

Finally, we note that every thing mentioned above applies to general graphs, but the subject of the current study is of a restricted class of graphs, namely:

Definition I.8. We say a graph is **regular** if every vertex has the same degree, and it is **d -regular** if that degree is d . A **cubic** graph is a 3-regular graph. It is not hard to see that a d -regular graph has $\frac{1}{2}d|V|$ edges, and so cubic graphs have $\frac{3}{2}|V|$ edges. As such, every cubic graph must have an even number of vertices.

D. Questions addressed in this paper

In this paper, we will restrict to only considering cubic graphs. All of the cubic graphs with N vertices have been enumerated up to $N = 40$, and datasets of these graphs are available online, e.g. <http://staffhome.ecm.uwa.edu.au/~00013890/remote/cubics/>.

Since these data files exist, we can do a comprehensive study of all cubic graphs of a certain order, and their ability to support patterns.

The main abstract questions that we address are as follows:

1. How many cubic graphs support patterns? A similar question: if we choose a cubic graph at random, what are the odds that it supports a pattern?
2. Are there graphs that support multiple patterns? If so, are these related?
3. Are there any graphs that support patterns with long links? If yes, is there a graph that supports multiple patterns, some of which have long links and some of which do not? How common are long-link patterns?
4. What can we say about the width of the basin of attraction of a pattern? Is there a connection between the width of this basin of attraction and the energy of a pattern? Is there a connection between this width and the linear stability of a pattern? Is there a connection between width and depth of a basin of attraction?

E. Methods

In this paper, we are finding attracting fixed points for a system of ODEs by a Monte Carlo method: we choose random initial conditions distributed uniformly in $[0, 2\pi]^{|V|}$ and flow (2) until the vector field approaches a fixed point (which we detect by observing the ℓ^2 norm of the vector field being less than 10^{-5}). We then double-check that this is a sink (and not a “slow saddle”) by numerically computing the eigenvalues of the Jacobian and verifying that it is negative semidefinite. In the simulations, there were only a tiny number of cases where the numerical Jacobian was needed because the system was trapped near a slow saddle. For a given stable pattern, we define the *spectral gap* of the pattern as the distance of the real part of the eigenvalue least negative real part from zero. Fixed points with large spectral gaps are in a sense “more stable” as perturbations decay more rapidly to the pattern.

This method both detects attracting fixed points and gives a statistical estimate of the width of the basin of attraction of a solution. For example, if we write S as the basin of a particular fixed point, then we can determine for any $z \in [0, 2\pi]^{|V|}$ if $z \in S$ or $z \notin S$. We then choose K_{samp} samples uniformly in the torus. The proportion of samples in S will converge to the normalized measure of S as $K_{\text{samp}} \rightarrow \infty$, and in fact this random proportion is normally distributed with variance $O(1/K_{\text{samp}})$, so that we could measure this set with whatever confidence we needed. Also note that this method will never give a false positive for a pattern, but patterns with small basins of attraction might be missed. For specific graphs of interest and that do not have too many nodes, it is possible to find *all* fixed points and assess their stability by using methods from computational algebraic geometry [MDDH15]. In the future, we hope to use their methods to study *interesting* graphs whose exact fixed points

cannot be readily found.

Finally, we use the enumerated datasets for the cubic graphs at the link mentioned above. For small enough $|V|$, we are thus able to consider every single cubic graph with $|V|$ vertices. In the last section of this paper, we discuss several specific graphs that have some interesting properties; e.g., the smallest cubic graph with a long link pattern.

II. GLOBAL STATISTICS

First note that we can show, just by exhaustive search, that there are graphs that support multiple patterns: in

$N \setminus k$	total cubics	no patterns	1 pattern	2 patterns	3 patterns	4 patterns	5	6	> 6
10	19	16	3						
12	85	61	22	2					
14	509	338	140	27	4				
16	4060	2038	1445	457	103	7			
18	41301	17658	13714	7048	2382	447	49	2	
20	9910*	2533	3565	2315	1088	333	66	9	1
30	1500*	8	53	130	245	265	257	203	339

TABLE I: Number of graphs supporting a particular number of patterns. The last two rows in this table represent a random sample of the possible graphs since there are 510,489 graphs for $N = 20$ and 845,480,228,069 graphs for $N = 30$. An exhaustive search would be expensive.

A. Fractions of patterns

For each N , there is $c(N) < \infty$, the total number of cubic graphs with N vertices. Let us define $f(N, k)$ as the proportion of these that support k distinct patterns.

We plot these results in Figures 1, 2, and 3. One thing that is clear is that for larger graphs, the fraction that support a pattern is growing.

In Figure 1, each curve corresponds to the fraction of graphs that support a certain number of patterns. We see from this data that each of these functions is increasing as a function of N .

In Figure 2, each curve corresponds to graphs with a certain number of vertices.

Finally, in Figure 3 we see that the fraction of graphs that contain a pattern is monotonically increasing as a function of the number of vertices. It is nearly linear and based on the small sample shown in table II, the plot will saturate at nearly 100 % when $N = 30$.

In Figure 4, we view all stable patterns for cubic graphs with $N = 16$ vertices. We are plotting several dimensions of data here: the energy of the pattern, the probability of it being attained, the spectral gap of a pattern (the absolute value of the negative eigenvalue closest to zero), and whether or not the pattern has a long edge. The line with slope $-3/2$ has been also added for comparison.

This figure has several salient features: first, we see that the patterns seem to fall into three clusters; second, inside each of these clusters, there is a strong (negative) correlation between the energy of a pattern and the width

of its basin of attraction; third, there is a strong correlation between the width of a basin of a pattern and its linear stability; fourth, long link solutions are quite common, but they tend to be higher in energy, harder to hit, and have smaller spectral gaps.

Also, we are careful not to be multiply counting patterns that are symmetries of each other; for example, any automorphism of G will move a stable pattern to another, and this one could look quite different numerically. However, one can see that any such automorphism will preserve the energy of a pattern as defined in (3) — so we require that two patterns have different energies before we consider them distinct.

In Figures 5 and 6, we plot the same as in Figure 4A, except these are graphs with $N = 18, N = 30$ vertices respectively. All of the same patterns apply, with the exception that there are now four clusters for $N = 30$.

III. STUDYING INDIVIDUAL GRAPHS

A. Explaining the clusters

We observed in several datasets above that the patterns seem to form a small number of clusters. For $N = 16, 18$ there were three, and for $N = 30$ there were four.

In Figure 7 we plot three graphs, one from each cluster.

The manner in which we plot these patterns is as follows: We first shift each solution so that $\theta_0 = 0$, and then plot the remaining θ 's at their angle in the plane. The radius is chosen to minimize collisions in the picture. We also color each vertex by angle, and edges are colored by black if short and red if long. Note that each of these graphs has a canonical “twist” count, which is the number of times the pattern wraps around the origin. It is very clear in the first two that the winding numbers are one and two, and in the third one can eventually pick out

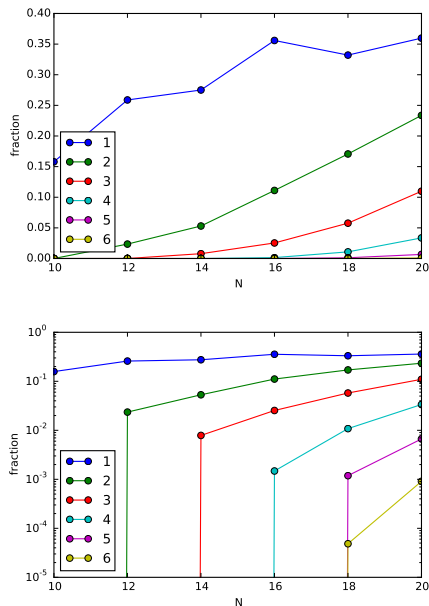


FIG. 1: We plot $f(N, k)$, where different curves correspond to different k and we plot versus N . The same data is plotted in both frames, one on a linear-linear scale, the other on a log-linear scale.

three distinct cycles around the origin: one twist is the inner diamond, one is the trapezoid with two red links, and finally there is a long independent cycle comprised entirely of short links. Each twist will add a particular amount of energy to the solution, which we bound below.

For example, assume that we have a twist consisting of m vertices around the circle; how much energy does this add to the solution? Assume that we have m vertices located at $0 = \theta_0 \leq \theta_1 \leq \dots \leq \theta_m = 2\pi$. Writing $\zeta_k = \theta_{k+1} - \theta_k$, we have that the energy added to the system by this loop is

$$F(\zeta) := \sum_{k=0}^{m-1} (1 - \cos(\zeta_k)),$$

with the constraints that $\zeta_k \in [0, 2\pi]$, $\sum_{k=0}^{m-1} \zeta_k = 2\pi$. Using Lagrange multipliers (or symmetry arguments), we see that the only interior optimizer is at the point $\zeta_k \equiv 2\pi/m$. The energy of such an equidistant loop is $m(1 - \cos(2\pi/m))$, a function whose maximum value (found at $m = 4$) is approximately 4. We see empirically that each loop tends to add about 3.5 to the total energy of the pattern. We note that for an isolated twist to be stable, it has to have at least 5 oscillators since the phase-difference between connected nodes should be smaller than $2\pi/4$. Thus, using $m = 5$ for the the energy of the minimal loop, we get 3.54 which is very close to the energy separating clusters. We note that this crude calculation sets an upper bound for the number of clusters to be roughly $N/5$. For $N = 14$ there are two clusters with energy difference of about 5.5 (data not shown).

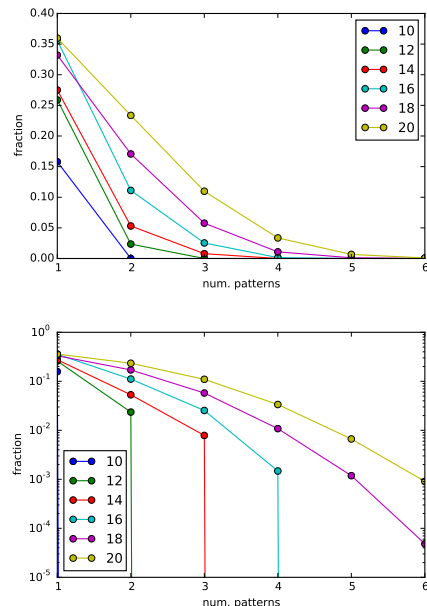


FIG. 2: We plot $f(N, k)$, where different curves correspond to different N and we plot versus k . The same data is plotted in both frames, one on a linear-linear scale, the other on a log-linear scale.

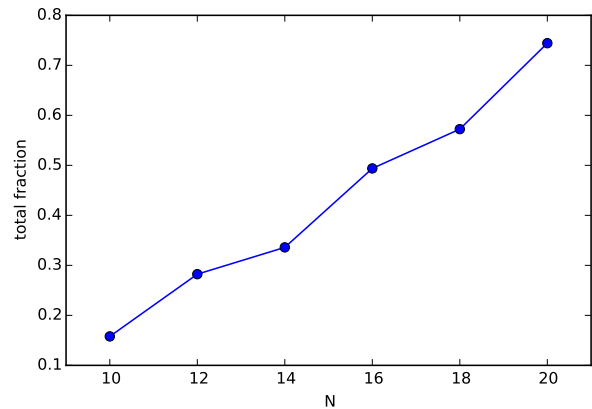


FIG. 3: We plot $\sum_k f(N, k)$, where different curves correspond to different N and we plot versus k .

B. Double ring graphs and their friends

The simplest example of a pattern on a cubic graph is two rings of length $N/2$ coupled to form a double ring. To construct this: label the nodes, $1, 2, \dots, N/2, N/2 + 1, \dots, N$. For nodes $1, \dots, N/2$, form a ring with nearest neighbor coupling (and 1 and $N/2$ connected) and similarly for nodes $N/2 + 1, \dots, 2N$. Then connect node j to $N/2 + j$ for $j = 1, \dots, N/2$. The pattern is then $\theta_j = 4\pi(j-1)/N$ for $j = 1, \dots, N/2$ and $\theta_j = \theta_{j-N/2}$ for $j = N/2, \dots, N$. If $N \geq 10$, the phase-difference between any pairs is less than $\pi/2$ in magnitude, so that

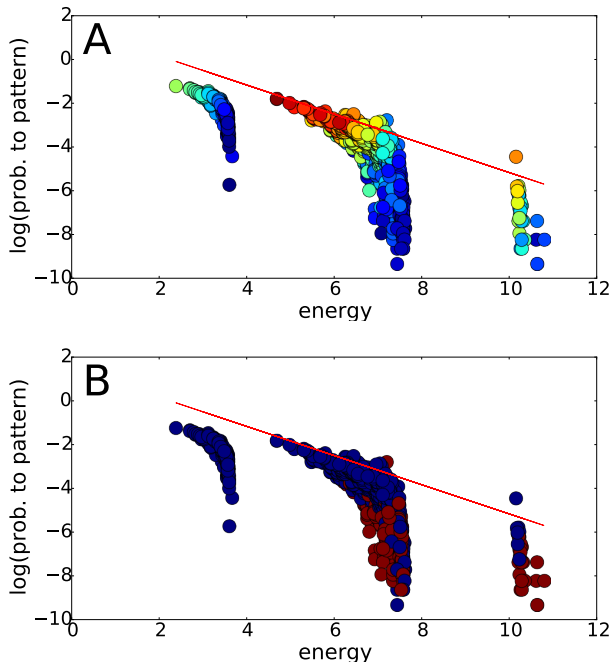


FIG. 4: Plot of all patterns for $N = 16$. The same data is plotted in both frames with a different coloring scheme. Each plotted circle corresponds to a single pattern; graphs with multiple patterns are represented by multiple dots in this plot. We plot the energy of each pattern versus the probability to decay to that pattern. In frame A the dots are colored by the spectral gap, which ranges from 0 (dark blue) to about 0.40 (red); in frame B we are simply coloring due to the presence of a long link: red represented a long link solution and blue a short link solution. The line corresponds to the function $\exp(-3/2(\text{energy}))$ which seems to be a nice empirical fit (we have no theory for this scaling).

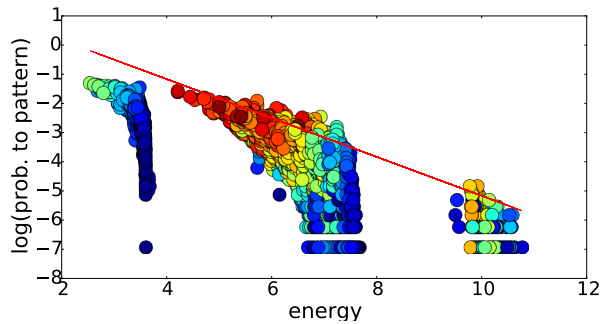


FIG. 5: Plot of all patterns for $N = 18$, same scheme used for Figure 4A.

the equilibrium will be stable. This result proves that there exists a cubic graph with N nodes that has a pattern for all $N \geq 10$. The double ring graph has energy $E = N(1 - \cos(4\pi/N))$; for $N = 18$, $E = 4.6863$ and this can be seen in figure 4 as the left most point in the second cluster. (The double ring has two twists, putting

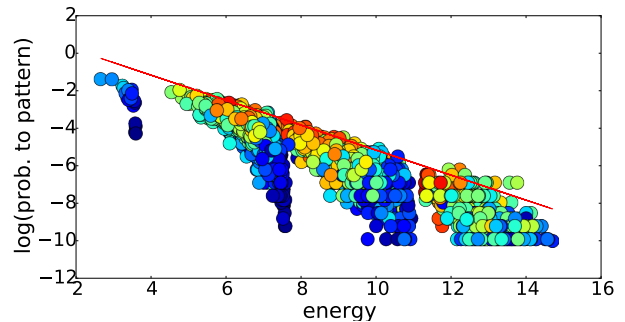


FIG. 6: Plot of all patterns for $N = 30$, same scheme used for Figure 4A.

it in the second cluster.)

C. $N = 10$

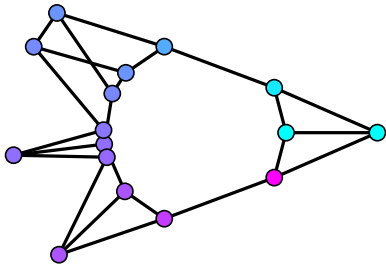
For ten-node cubic graphs there are only three graphs that have patterns and each of these has a single pattern. They are illustrated in figure 8. The left most is the double-ring graph; the middle is a Möbius-strip but has the same phase relations as the double ring. Both these graphs seem to have a similar basin and they have exactly the same energy since all phase-differences are the same. (Note that the Moebius graph has the obvious generalization for all $N \geq 10$ similar to the double-ring construction above.)

The right-most graph is also quite close to the double ring graph, but the two pairs of nodes have swapped connections. This graph has a much smaller basin of attraction (and larger energy) than does the double ring graph. Let us consider the analogue of this twisted graph with more vertices. Let $N = 2m$. Let b_m be the root of the function

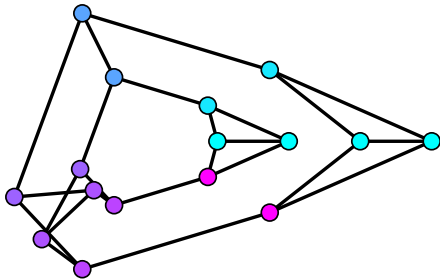
$$g(b) = 2 \sin((m-1)b) + \sin(b)$$

that lies between $2\pi/m$ and $2\pi/(m-1)$. It is clear that for $m > 4$ that $g(2\pi/(m-1)) > 0$ and $g(2\pi/m) < 0$ so by continuity such a root exists. We now define the phases around the twisted circle graph that consists of two rings of m nodes. We consider $m = 2k+1$ and $m = 2k$ separately. We connect the nodes in each ring exactly as in the double ring. Next, writing, $m = 2k+1$, swap the k^{th} and $(k+1)^{\text{th}}$ connections between the rings to form the twisted graph. Now assign the phases of the pattern as follows: inner and outer nodes $j = 0, \dots, k$ are assigned jb_m ; nodes $j = k+1, \dots, 2k$ are assigned $-(m-j)b_m$. This is a phase-locked pattern as long as $g(b_m) = 0$. (That is the sum of all phase-differences between connected pairs is zero.) The possible phase-differences between any pairs are $0, \pm b_m, \pm(m-1)b_m$. Our bounds on the root b_m assure that the cosine of each phase-difference is positive as long as $m > 4$. Thus, that pattern is stable. For m even, we label the rings

Graph number 528, Energy = 3.408, SG = 0.103



Graph number 313, Energy = 7.432, SG = 0.029



Graph number 4028, Energy = 10.278, SG = 0.159

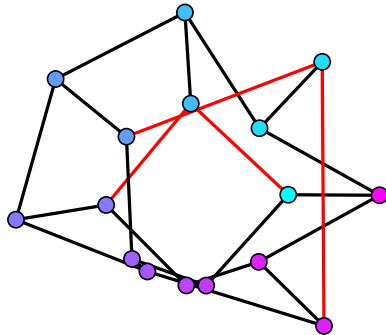


FIG. 7: $N = 16$, one graph from each cluster.

as with the odd case and assign phases on each ring as $0, b_m, \dots, (k-1)b_m, -kb_m, -(k-1)b_m, \dots, -b_m$. This leads to phase differences between connected pairs that are either $0, \pm b_m$, or $\pm(m-1)b_m$. Existence and stability are as with the odd case. This and the previous section show that for any number of nodes $N \geq 10$ there are at least three cubic graphs that have simple stable patterns that are qualitatively like the traveling wave on a ring of $N/2$ nodes.

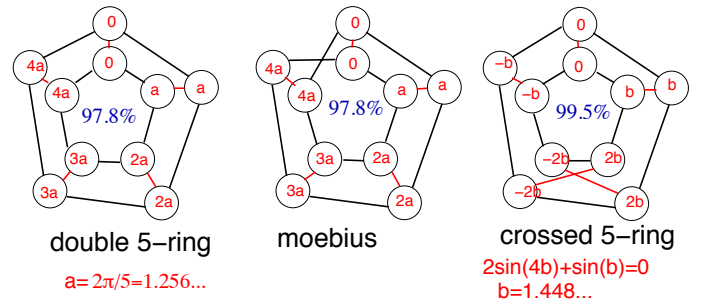


FIG. 8: The three cubic graphs of 10 nodes that admit patterns. Relative phases are labels a, b and the fraction of simulations that lead to synchronization is in blue. (That is, only about 2% of simulations lead to the pattern shown in the left two and 0.5% in the right-most graph.) The left-most graph is the double ring graph for $N = 10$. The middle is a kind of Möbius-strip graph and has the same fixed point and basin width as the double ring. The right-most graph is also like the double-ring, but two of the links are crossed. The value of the phase, b is close to, but slightly larger, than $a = 2\pi/5$. The phase-difference of $2\pi - 4b$ is thus less than $2\pi - 4a$ and so is still a short link.

D. $N = 12$ with long links

For $N = 12$ there are 24/88 graphs that support patterns. $N = 12$ is also the lowest number of nodes for which there are patterns with long links. Recall long links are those where the phase-difference exceeds $\pi/2$. Of the 24 graphs with stable patterns, 4 of them have patterns with long links and of these 4 graphs, 3 of them have phase-differences that are very close to $\pi/2$, so the links are nearly neutral ($\cos(\phi) = 0$). However, one graph has a link where the phase-difference is quite large and we now discuss this graph (we will call it G_{50} since was the 50th graph in the database of 12 node cubic graphs referenced in Section I D) as it has some interesting properties. It is illustrated in figure 9A and has been drawn in such a way that one can see the relationship between it and the double 6-ring graph. First, if the links drawn with the blue X's are deleted and the dashed blue links are added instead, we recover the double 6-ring graph and the corresponding phases are given in the nodes and outside the nodes in blue, when they differ from those in G_{50} . In this case, the value of a will be $2\pi/6$. On the other hand, the phases for G_{50} are not so symmetric, but are still simple and can be defined by two numbers, a and b . By looking at the summed sines of the phase-differences, it can be seen that if there is such a pattern, we must have $\sin(b-a) = 2\sin(a)$ and $\sin(b-a) = \sin(b)$. We can use Maple or some other symbolic algebra package to see that

$$a = 2\sin^{-1}(1/4) \approx 0.50536,$$

$$b = \pi - \tan^{-1}\sqrt{15} \approx 1.8235,$$

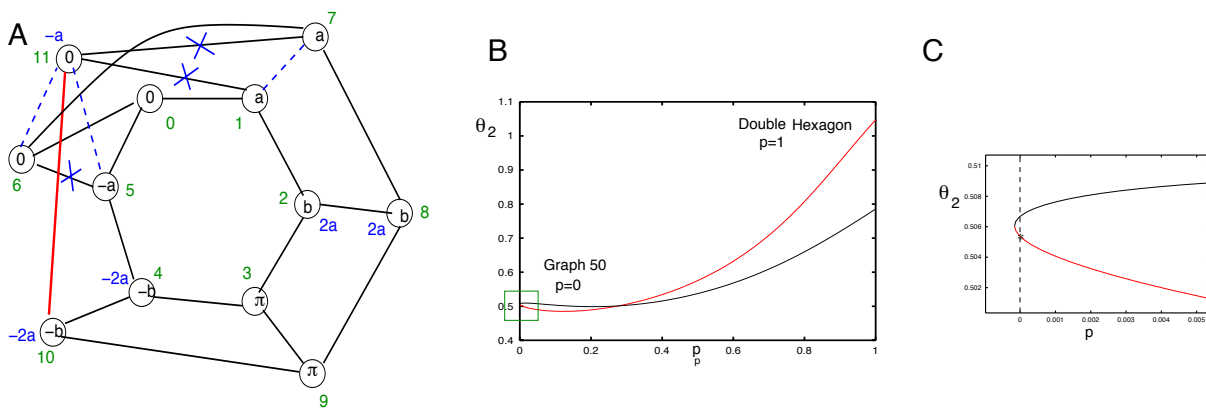


FIG. 9: A 12-node graph (G_{50}) with a long link pattern. (A) The graph and its pattern of phases (long link is shown in red) also showing that it is similar to the double-ring graph with 12 nodes. Removal of the X-ed out links and replacing them with the dashed links leads to the double ring graph whose phases are shown in blue. (B) Numerical continuation of the pattern on the double-ring ($p = 1$) to the pattern on G_{50} ($p = 0$) and an expanded view (C).

so, in particular, $b > \pi/2$. We see that the long link occurs between nodes 10 and 11. Since there are only three connections that are different between this graph and the double ring, we can start with the double ring graph pattern and use continuation to homotopy to G_{50} . Figures 9B,C show that the pattern on the double ring is continuously deformed to the long-link pattern on G_{50} . Note that the limit point or fold occurs very close to $p = 0$, showing that the pattern on G_{50} has an eigenvalue very near zero. We also see in the bifurcation diagram of 9C that there is a saddle-node bifurcation for p a bit less than zero. This saddle plays a significant role in the dynamics of Kuramoto oscillators when noise is added. For example, the energy difference between the nearest saddle and the sink is the quantity that governs the mean escape time away from the sink; more precisely, if we force (2) with white noise of amplitude $\sqrt{2\epsilon}$, then the mean escape time out of this pattern would be

$$\mathbb{E}[\tau] \asymp \exp(\epsilon^{-1}(\Phi_G(\text{saddle}) - \Phi_G(\text{sink}))).$$

We have not been able to study this systematically for all of the graphs considered in this paper, but we have seen a strong correlation in the numerics between three properties for any particular pattern: (i) the Jacobian at the pattern having a small spectral gap; (ii) the basin of attraction of the pattern being small; (iii) the potential height needed to escape the basin of attraction of the pattern.

In fact, we conjecture that for any pattern, if any of these are small, then the other two must be. We can see the correlation between (i) and (ii) in Figures 4 and 6: there is a clear pattern that as we move vertically down in the graph, the points become closer to blue. Similarly, we see that (ii) and (iii) are correlated in at least the G_{50} vs. double hex graph, in that the double hex graph has a much larger basin of attraction.

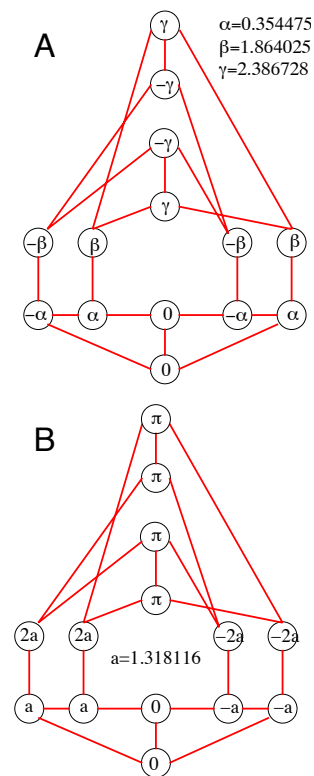


FIG. 10: A Graph with two patterns. (A) The higher energy patterns depends on the parameters α, β with $2\gamma + \beta - \alpha = 2\pi$. (Equations for α, β are in the text.) (B) The low energy pattern depends on the parameter $a = \cos^{-1}(1/4)$.

E. A graph with multiple patterns.

$N = 12$ is also the first instance that indicates a graph with more than one possible pattern; there appear to be two such graphs. However, the patterns on these graphs are complex and there is very little difference in their

energies; the exact phases cannot be easily determined analytically, so we turn to a particular example with $N = 14$. Figure 10 shows such a graph with its two patterns shown in A,B. The low energy pattern (panel B) depends on only one parameter that satisfies $2\sin(2a) - \sin(a) = 0$ which leads to $a = \cos^{-1}(1/4)$. The higher energy pattern shown in panel A depends on two parameters, α, β and satisfy:

$$\begin{aligned} 0 &= \sin(\beta - \alpha) - \sin(2\alpha) - \sin(\alpha) \\ 0 &= \sin(\beta - \alpha) - 2\sin(3\beta/2 - \alpha/2) \end{aligned}$$

which can be solved numerically to yield two nontrivial solutions. One of these solutions leads to an unstable equilibrium, but one is stable, and this is shown in panel A. The lower energy pattern ($E = 7.0$) appears in 1.706% of the simulations and the higher energy ($E = 7.43$) appears in 0.291% of the simulations; all other simulations lead to synchrony.

F. High energy patterns.

Let us define

$$\begin{aligned} E_N &= 10 \left[\frac{N}{10} \right] (1 - \cos(2\pi/5)), \\ F_N &= 10 \left[\frac{N}{10} \right] (8(1 - \cos(\beta^*)) + 4(1 - \cos(4\beta^*))), \end{aligned}$$

where β^* is the root of $2\sin(4x) + \sin(x)$ that lies between $2\pi/5$ and $\pi/2$. Then we will show in this section that for every $N \geq 10$, there is a pattern with energy E_N , and for any $N = 10m$ with $m \geq 1$, there is a pattern with energy F_N . Note that the second statement is always stronger, since

$$\frac{E_{10m}}{10m} \approx 6.90983, \quad \frac{F_{10m}}{10m} \approx 7.49165.$$

The proof for the F_{10m} energy is simpler. Consider the crossed 5-ring in Figure 8, where we number the outside vertices $1, \dots, 5$ and the inside vertices $6, \dots, 10$, so that $i \leftrightarrow i + 5$. Consider m disjoint copies of this graph, with vertices labeled j, k , with $j = 1, \dots, m$ and $k \in 1, \dots, 10$. Now rewire these graphs as follows: remove the edges $1.1 \leftrightarrow 1.6$ and $2.1 \leftrightarrow 2.6$ and cross them up as $2.1 \leftrightarrow 1.6$ and $1.1 \leftrightarrow 2.6$. If $m \geq 3$, do the similar crossing with $2.2 \leftrightarrow 2.7$ and $3.2 \leftrightarrow 3.7$, etc. Each vertex is still degree three, and the pattern is still the same, since we have only disconnected and reconnected vertices with the same angle. We also see that this pattern has energy F_{10m} .

Now we show that there are stable patterns with energy E_N for all $N \geq 2$. We first describe the construction for $N = 10m$. Create $2m$ 5-ring graphs. These are disjoint and we label their vertices A, B, C, D, E . Put the 5-wave on each one so that vertex A has phase 0, B has phase $2\pi/5$, etc. Clearly the energy from each ring is $5(1 - \cos(2\pi/5))$ and the total energy at this point is

E_N . Choose some pairing of the $2m$ rings into m pairs, and connect the A vertices between the two rings in each pair. Choose a different pairing of the $2m$ rings, and connect the B vertices, etc. Go all the way until the E vertices. Notice that the connections that came from the pairings only couple nodes at the same angle, so these new pairings contribute neither to the vector field (2) or the energy (3). Therefore we still have a fixed point with energy E_N . Also notice that each node has degree three: connected to two nodes in the original rings, and one more connection in these pairings. We can also see that there are choices which give a connected graph: if we label the original rings $1, \dots, m$ and $1', \dots, m'$, and choose the A pairing to be $i \leftrightarrow i'$ and the B pairing to be $i \leftrightarrow (i + 1)'$, then the entire graph will be connected at that stage (for example, there is a path in the rings that goes as $1 \rightarrow 2' \rightarrow 2 \rightarrow 3' \rightarrow 3 \rightarrow \dots$ and the rings are connected).

One can construct graphs with energy E_N in a similar manner for the in-between cases, i.e. $10m < N < 10(m + 1)$ where $m \geq 2$. Let us write $k = N - 10m$, noting that it is even and less than 10. Let us write $k/2$ pairs of nodes labeled A', B' , using whichever letters are necessary. Construct the $10m$ vertex graph from $2m$ rings described above. Choose any two pairs of A vertices that were connected in the last step above, call them $A_1 \leftrightarrow A_2$ and $A_3 \leftrightarrow A_4$. Break these two connections, and add the edges

$$A'_1 \leftrightarrow A_1, A_3, \quad A'_2 \leftrightarrow A_2, A_4, \quad A'_1 \leftrightarrow A'_2.$$

Note that each of the four A_i vertices have had one edge removed and one edge reconnected, so are still degree 3, and note that by construction A'_i each have degree three. Thus we now have $10m + 2$ vertices in the cubic graph which support the same pattern and energy E_m . We can repeat this construction as necessary through B', C' , etc.

We see directly that F_{10} is the maximal energy for $N = 10$, and we have not observed any higher energies in the simulations presented in Section II. For $N = 20$, the highest energy observed by random search has energy less than 11, yet $E_{20} = 13.82$ and similarly the highest energy we saw for $N = 30$ was less than 15, yet $E_{30} = 20.72$. The reason for this is that our sampling of graphs was not exhaustive and so there is a low probability that these special graphs would be chosen. Furthermore, the actual pattern seems to have a small basin of attraction. For $N = 20$, we constructed a graph using the algorithm above that had energy E_{20} . We ran simulations with 20000 random initial conditions and the energy E_{20} showed up 3 times. (There were two other patterns that have much lower energies and occur with a probabilities, 13% and 0.6%.) Thus, these high energy patterns seem to have a small basin of attraction even when they do exist. And this actually makes sense: the stable pattern has a very specific choice of angles and twists around certain cycles, and it seems unlikely that any initial condition that decayed to it would have to have the same winding index on all of these cycles.

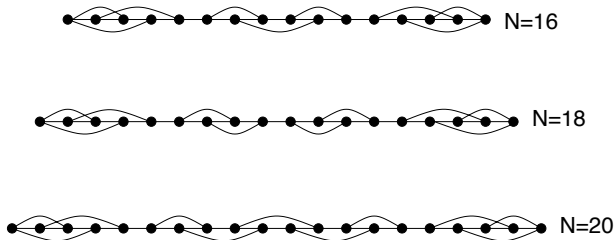


FIG. 11:

G. Graphs with no patterns.

As our statistics have shown, as N gets larger, it seems that there will be a larger and larger fraction of graphs that have patterns and this fraction tends to 1. That means, in particular, that graphs with no patterns are increasingly rare. We can construct graphs that seem to have no patterns for any N by starting with the linear chain of N nodes with nearest neighbor coupling. The two end nodes are deficient by two edges and the remaining are deficient by 1. The strategy is to connect the nodes in such a way as to preclude any cycles that contain 5 or more nodes and such that within those cycles there are no shortcuts. That is the shortest path to any node in the cycle requires going on the cycle. Figure 11 shows three graphs for $N = 16, 18, 20$. The algorithm involves finishing off the edges first so that there are $N - 10$ edges remaining. (Each edge takes 5 nodes.) Finish the remaining interior nodes by adding paths that are either two or three oscillators away. No cycle contains more than 4 nodes. (There are longer cycles in the graphs, but there are shortcuts between nodes in the cycle.) In unpublished work with Dhaghash Mehta, we have used the methods in [MDDH15] to show that the three graphs illustrate in the figure have no patterns. We conjecture that graphs of this form (which exist for all $N \geq 10$) have no patterns. If one ignores everything but the nearest neighbor connections, then it is easy to show that the only phase-differences are $0, \pm\pi$ and only 0 is stable.

IV. CONCLUSIONS

We have presented the results of a systematic computation on the existence and properties of non-trivial phase-locked patterns for the Kuramoto oscillator on a cubic graph.

The main observations are that cubic graphs can in general support a wide variety of patterns when there are enough vertices. We even have a graph in the dataset that supports twelve distinct patterns (one example with $N = 30$), but graphs that support multiple patterns are quite common, see Table II. The data also seems to suggest that as N increases, the probability of a randomly chosen cubic graph with N vertices not being able to support a pattern asymptotes to zero.

We have also seen that there are a large number of graphs that support a pattern with long links, q.v. Figure 4. In fact, about one quarter of the patterns observed for $N = 16$ are “long link” patterns. In some sense, the search for such patterns is what motivated the current study, as it is known that the all-to-all graph [MS90] and the ring graph [DeV12] do not have any such patterns, yet the results of [BDJP12] show that it is possible for a long-link pattern to be linearly stable. In the event, we have discovered that they are actually quite common.

We have also shown strong numerical evidence that there is a correlation between the width of a basin of attraction and its linear stability (in Figures 4, 6, the datapoints get more blue as we move down in probability). We have also discovered that there is a (negative) correlation between this and the energy of the pattern, but it is somewhat complicated. In those figures, we see that all of the patterns form clusters based on their winding number, and inside each cluster there is a pretty strong negative correlation between energy and width of the basin. We also see in some particular cases a connection between the width of a basin of attraction and its depth, and conjecture that this relation holds more generally.

However, we see that this study raises more questions than it answers. It would be interesting to make progress on proving the conjecture stated in Section III D. Another question would be if we could determine whether or not a graph would support a pattern based on some general properties of a graph — as we mention above, one can eliminate the possibility for a graph to sustain a pattern when it lacks certain structures. But the only analytic technique we know to show that a graph will support a pattern is the type of hands-on analysis done in Section III.

Another interesting question is whether graphs denser than cubic graphs will have the same propensity for patterns and also for long-link patterns as we have seen here. Adding edges can really have opposing effects when it comes to the stability of a pattern: more edges means more loops, but it also means more constraints pulling a pattern in more directions. One natural direction of future research is to study more general graphs to try and predict the relationship of a graphs propensity to support patterns with some gross graph statistics, e.g. average degree, average clustering coefficient, etc.

V. ACKNOWLEDGMENTS

We would like to thank Dhaghash Mehta and Jonathan Hauenstein for computing the all fixed points for the graphs in figure 11. We would also like to thank summer student Ethan Levien for some early computations of non-synchronized attractors in the small cubic graphs. B.E. was supported by NSF grant DMS 1219753; L. D. was supported by the National Aeronautics and Space Administration (NASA) through the NASA Astrobi-

ology Institute under Cooperative Agreement Number NNA13AA91A issued through the Science Mission Di-

rectorate.

-
- [AC13] John-Mark A Allen and MC Cross, *Frequency precision of two-dimensional lattices of coupled oscillators with spiral patterns*, Physical Review E **87** (2013), no. 5, 052902.
- [BD14] Jared Bronski and Lee DeVille, *Spectral theory for dynamics on graphs containing attractive and repulsive interactions*, SIAM J. Appl. Math. **74** (2014), no. 1, 83–105.
- [BDF] Jared Bronski, Lee DeVille, and Timothy Ferguson, *Graph homology and stability of coupled oscillator networks*, submitted August 2015.
- [BDJP12] Jared C. Bronski, Lee DeVille, and Moon Jip Park, *Fully synchronous solutions and the synchronization phase transition for the finite- n kuramoto model*, Chaos **22** (2012), no. 3, 033133.
- [BDK] Jared Bronski, Lee DeVille, and Paolina Koutsaki, *The spectral index of signed laplacians and their structural stability*, submitted March 2015.
- [CHR82] Avis H Cohen, Philip J Holmes, and Richard H Rand, *The nature of the coupling between segmental oscillators of the lamprey spinal generator for locomotion: a mathematical model*, Journal of mathematical biology **13** (1982), no. 3, 345–369.
- [Chu97] F.R.K. Chung, *Spectral Graph Theory (CBMS Regional Conference Series in Mathematics, no. 92)*, American Mathematical Society, 1997.
- [DeV12] Lee DeVille, *Transitions amongst synchronous solutions in the stochastic kuramoto model*, Nonlinearity **25** (2012), no. 5, 1473–1494.
- [EK84] G. B. Ermentrout and N. Kopell, *Frequency plateaus in a chain of weakly coupled oscillators, I.*, SIAM Journal on Mathematical Analysis **15** (1984), no. 2, 215–237.
- [EK01] G Bard Ermentrout and David Kleinfeld, *Traveling electrical waves in cortex: insights from phase dynamics and speculation on a computational role*, Neuron **29** (2001), no. 1, 33–44.
- [Erm92] G Bard Ermentrout, *Stable periodic solutions to discrete and continuum arrays of weakly coupled nonlinear oscillators*, SIAM Journal on Applied Mathematics **52** (1992), no. 6, 1665–1687.
- [GS06] Martin Golubitsky and Ian Stewart, *Nonlinear dynamics of networks: the groupoid formalism*, Bull. Amer. Math. Soc. (N.S.) **43** (2006), no. 3, 305–364. MR 2223010 (2008k:37182)
- [MDDH15] Dhagash Mehta, Noah S Daleo, Florian Dörfler, and Jonathan D Hauenstein, *Algebraic geometrization of the kuramoto model: Equilibria and stability analysis*, Chaos: An Interdisciplinary Journal of Nonlinear Science **25** (2015), no. 5, 053103.
- [MS90] R. E. Mirollo and S. H. Strogatz, *Synchronization of pulse-coupled biological oscillators*, SIAM J. Appl. Math. **50** (1990), no. 6, 1645–1662. MR MR1080514 (91m:92012)
- [PE94] Joseph E Paultet and G Bard Ermentrout, *Stable rotating waves in two-dimensional discrete active media*, SIAM Journal on Applied Mathematics **54** (1994), no. 6, 1720–1744.
- [Str00] Steven H. Strogatz, *From Kuramoto to Crawford: exploring the onset of synchronization in populations of coupled oscillators*, Phys. D **143** (2000), no. 1-4, 1–20, Bifurcations, patterns and symmetry. MR 1783382 (2001g:82008)
- [UE15] Lawrence C Udeigwe and G Bard Ermentrout, *Waves and patterns on regular graphs*, SIAM Journal on Applied Dynamical Systems **14** (2015), no. 2, 1102–1129.
- [WSG06] D.A. Wiley, S.H. Strogatz, and M. Girvan, *The size of the sync basin*, Chaos: An Interdisciplinary Journal of Nonlinear Science **16** (2006), 015103.